

Growth of single-crystalline rutile TiO₂ nanorods on fluorine-doped tin oxide glass for organic–inorganic hybrid solar cells

Junting Xi · Orawan Wiranwetchayan ·
Qifeng Zhang · Zhiqiang Liang · Yueming Sun ·
Guozhong Cao

Received: 6 November 2011 / Accepted: 30 January 2012 / Published online: 16 February 2012
© Springer Science+Business Media, LLC 2012

Abstract Single-crystalline TiO₂ nanorods (TiO₂ NRs) are grown directly on FTO substrates by hydrothermal methods. The diameters and lengths of TiO₂ NRs are easily controlled by growth conditions. When used in hybrid solar cells, TiO₂ NRs function as the continuous pathway for fast electron transport to charge collecting electrode, demonstrating a high power conversion efficiency (PCE) of 3.21% with 140 nm long TiO₂ NRs. The bilayer polymer coating are introduced into 500 nm long TiO₂ NRs to reduce the surface roughness, resulting in the improved contact between the polymer blend and silver electrode and an enhanced PCE from 2.70 to 3.07%.

1 Introduction

Organic photovoltaics (OPVs) have attracted much attention because of their potential for light-weight, flexibility, low-cost manufacturing and large-area conversion of solar energy to electricity [1–3]. One of the intrinsic drawbacks of OPVs, which limits OPVs from achieving higher power conversion efficiency (PCE), is the short diffusion length of excitons (pairs of a hole and an electron), typically around 20 nm. To alleviate the impact of short diffusion length of excitons, bulk heterojunction (BHJ), which is based on two interpenetrating networks of respective *p*-type electron

donor and *n*-type acceptor, has been widely applied in the OPVs [4–6]. The BHJ structure ensures the plentiful interfacial area for photo-generated excitons to dissociate. Although the recent work on a new benzodithiophene polymer (PTB7)/phenyl-C71-butyric acid methyl ester (PC71BM) OPVs achieved a highest PCE of 7.4% [7]. The most commonly used *p*-type donor and *n*-type acceptor polymers are poly (3-hexyl-thiophene) (P3HT) and [6, 6]-phenyl-C61-butyric acid methyl ester (PCBM), respectively, and the PCE of 4–5% have been reported [3, 8–11]. Another factor that limits achieving higher PCE in OPVs is the inefficient carrier transport due to the low charge mobility of polymer [12]. Inorganic semiconductors, with much higher charge mobility, such as TiO₂, [9, 12–14] ZnO, [2, 3, 15] and CdS [2] have been explored and studied to overcome this shortcoming, and used in organic/inorganic hybrid solar cells. In addition, such inorganic semiconductors, when appropriately incorporated into the solar cell structures, have demonstrated the ability to significantly improve the physical and chemical stability of the resulting hybrid solar cells, leading to a much longer life time of the solar cells [16]. However, the full potential of the organic–inorganic hybrid solar cells has been suppressed so far with a relatively lower PCE as compared to their counterpart OPVs, due at least in part to the poor contact at the organic/inorganic interfaces. One approach to improve the photovoltaic performance of hybrid solar cells is to incorporate a functional interlayer to improve the electronic junction between the organic/inorganic interfaces [3, 15, 16]. A fullerene-based self-assembled monolayer was introduced into the TiO₂ and ZnO based hybrid solar cells, which affected charge transfer at the interface to reduce the recombination, and passivated surface trap states of inorganic semiconductors, resulting in much enhanced performance [16].

J. Xi · Y. Sun (✉)
School of Chemistry and Chemical Engineering,
Southeast University, Nanjing 211189, Jiangsu, China
e-mail: sun@seu.edu.cn

J. Xi · O. Wiranwetchayan · Q. Zhang · Z. Liang · G. Cao (✉)
Department of Materials Science and Engineering,
University of Washington, Seattle, WA 98195, USA
e-mail: gzcao@u.washington.edu

In comparison with the double-layer heterostructure based on inorganic nanoparticles, the hybrid solar cells based on ordered or well aligned nanowires/nanotubes have the advantages of large donor–acceptor interface for excitons to dissociate, excellent electron mobility and direct pathway for easy electron transport to reduce the electron recombination, which can significantly increase the PCE of the devices [1, 9, 12]. ZnO nanorod arrays were applied in hybrid solar cells first, and the highest PCE achieved was up to 2.7% [17], demonstrated the important role of ZnO nanorod array in collecting photogenerated electrons and acting as the conducting path to the electrode. Wei et al. [18] and Kuo et al. [12] had successfully synthesized vertically aligned TiO₂ nanorods for hybrid solar cells, also proved the enhancement of PCE as compared to the dense TiO₂ film. However, the performances of hybrid solar cells based on TiO₂/ZnO nanorods remain low; especially hybrid solar cells based on TiO₂ NRs achieved less than 1% PCE. This relatively low PCE may be partly attributed to poor crystallinity of TiO₂ nanorod arrays as they were fabricated using templates or with seeding.

This paper reports the growth of single-crystalline rutile TiO₂ nanorods (NRs) directly on fluorine-doped tin oxide (FTO) substrates by means of hydrothermal method with the diameters and lengths of TiO₂ NRs easily controlled by the growth conditions. This method is technically straightforward and reliable, and the resulting TiO₂ nanorods are directly grown from the FTO substrate without using either templates or seeds. When used in hybrid solar cells, TiO₂ NRs function as the continuous pathway for fast electron transport to charge collecting electrode, demonstrating a high power conversion efficiency (PCE) of 3.21% with 140 nm long TiO₂ NRs while the reference hybrid solar cells based on TiO₂ DF shows a PCE of 2.79%. The bilayer polymer coating are introduced into 500 nm long TiO₂ NRs to reduce the surface roughness, resulting in the improved contact between the polymer blend and silver electrode and an enhanced PCE from 2.70 to 3.07%.

2 Experimental

TiO₂ NRs were grown directly on FTO substrates by means of hydrothermal methods; similarly grown TiO₂ NRs have been studied in dye-sensitized solar cells [19–21]. Briefly, 0.5 ml titanium butoxide (Sigma-Aldrich) was added into a mixture of DI water and concentrated (36%) hydrochloric acid (HCl) with a volume ratio of 1:1. After stirring at ambient conditions for 5 min, the solution became clear and transparent. The resulting solution was then transferred into the autoclave in which the FTO substrates were placed at an angle against the wall of the Teflon-liner. The autoclave was placed in an oven preheated to 150 °C for a pre-determined

duration. After the synthesis, the autoclave was cooled down naturally to room temperature. The sample was rinsed with DI water thoroughly, followed by annealing at 450 °C in air for 1 h. The diameters and lengths of TiO₂ NRs could be controlled by varying the growth time. Two different types of TiO₂ NRs presented in this work were grown at 150 °C for 85 min (labeled as TiO₂ NRs 1) and 100 min (labeled as TiO₂ NRs 2), respectively.

A multilayer hybrid solar cell based on the configuration FTO/TiO₂ NRs/PCBM/P3HT: PCBM/PEDOT: PSS/Ag was fabricated. Firstly, the PCBM interlayer was spin-coated from a dichloromethane solution containing 20 mg/ml of PCBM onto the TiO₂ NRs at a rate of 1,000 rpm for 30 s. Secondly, the P3HT/PCBM blend solution with a concentration ratio of 1:0.8 in chlorobenzene, was spin-coated at the same rate for another 30 s. Finally, a hole-transport layer of poly (3, 4-ethylene-dioxythiophene)-poly (styrene sulfonic acid) (PEDOT: PSS) was deposited on the top, followed by thermally evaporated of silver as the anode. The bilayer polymer coated TiO₂ NRs 2 (TiO₂ NRs 2-DL) was prepared by spin-coating two layers of P3HT/PCBM blend solution to reduce the surface roughness before evaporating the anode, under otherwise identical fabrication conditions. Typical active areas for photovoltaic devices are 3.14 mm².

Reference solar cells based on TiO₂ dense film (TiO₂ DF), using an FTO/TiO₂ DF/PCBM/P3HT: PCBM/PEDOT: PSS/Ag configuration, were prepared with the same fabrication procedure under identical fabrication conditions. TiO₂ dense film was prepared by spin-coating TiO₂ sol on FTO substrates, followed with heat treatment at 450 °C in air for 1 h. TiO₂ sol was obtained by hydrolyzing titanium alkoxide in an acidic aqueous. Typically, 1 mL of titanium isopropoxide was added to 20 mL of distilled water containing 0.5 mL of hydrochloric acid. A white precipitate appeared in the beginning. After stirring for about 30 min, the precipitate completely dissolved, resulting in the formation of a TiO₂ sol in light yellow color.

The J-V characteristics of the photovoltaic devices were tested inside a N₂ filled glove box using a Keithley 2,400 source measurement unit, and an Oriel Xenon lamp (450 W) coupled with an AM1.5 filter. The light intensity was calibrated with a standard silicon solar cell certificated by the National Renewable Energy Laboratory to confirm the measurement conditions. A light intensity of 100 mW/cm² was used in all the measurements in this study.

3 Discussions

Figure 1a and c are the top-view scanning electron microscopy (SEM) images of TiO₂ NRs 1 and TiO₂ NRs 2,

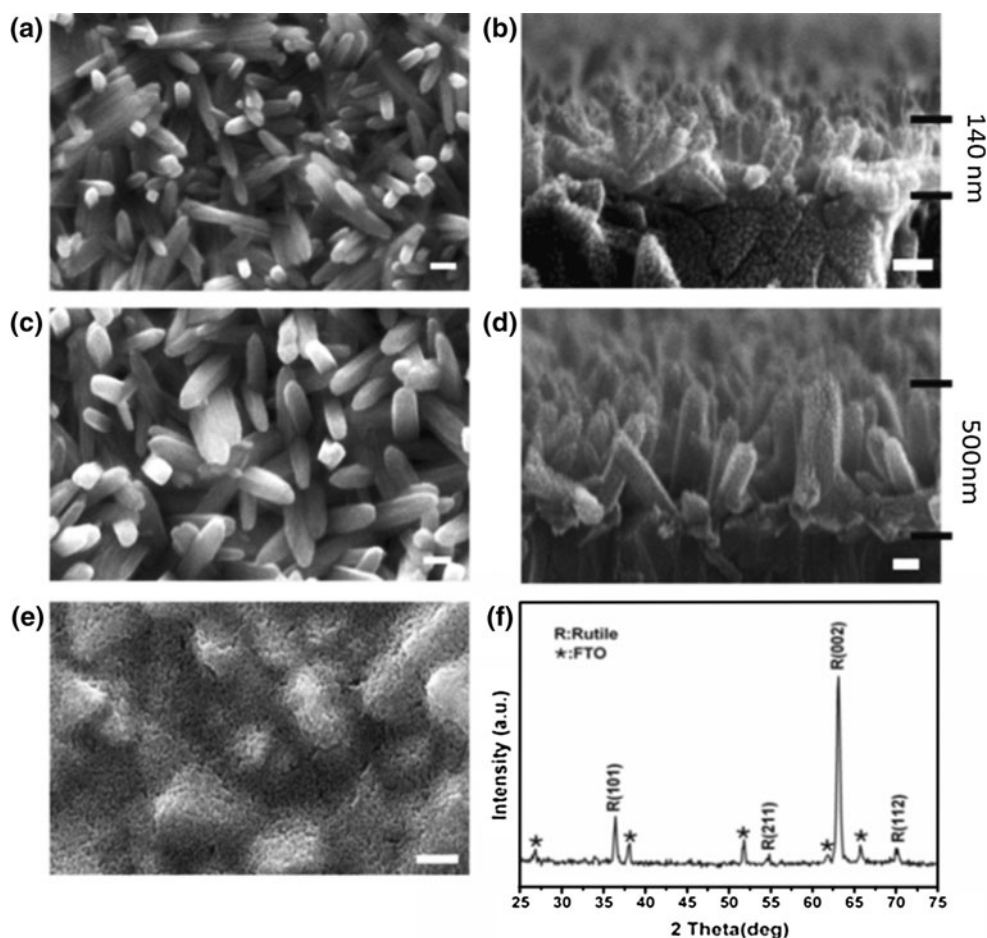
respectively. Figure 1b and d show the cross-section of TiO₂ NRs 1 and TiO₂ NRs 2. Both diameters and lengths of TiO₂ NRs increased with increasing reaction time. TiO₂ NRs 1 sample grown at 150 °C for 85 min has diameters of 50 ± 15 nm (Fig. 1a). When the growth time increased to 100 min, the diameters of the resultant TiO₂ NRs 2 increased to 75 ± 15 nm (Fig. 1c). The lengths of TiO₂ NRs were also found to change from ~140 nm (TiO₂ NRs 1, shown in Fig. 1b) to ~500 nm (TiO₂ NRs 2, Fig. 1d), with better vertical alignment. It should be noted that there seems to be a long incubation time before the growth of TiO₂ nanorods on the FTO substrate. It is not clear at this moment if such a long incubation time is related to initial heterogeneous nucleation on the FTO substrate surface. Figure 1f shows the X-ray diffraction (XRD) pattern of TiO₂ NRs on FTO substrate. All the diffraction peaks agreed well with that of the rutile phase and the FTO substrate marked with asterisks.

A multilayer hybrid solar cell based on TiO₂ NRs was fabricated as schematically illustrated in Fig. 2a. TiO₂ NRs are filled with the PCBM interlayer first and then the blend of P3HT and PCBM as a photoelectrode in hybrid solar cells. The PCBM interlayer can enhance electrical

coherence at the blend polymer/TiO₂ NRs interfaces [15]. The BHJ structure provides the sufficient interfacial area for the quick separation of photogenerated excitons. The single crystalline TiO₂ NRs can function as the direct pathway for the fast and smooth electron transport to the charge collecting electrode, which will be helpful to suppress hole/electron recombination. And a simplified energy level diagram of the TiO₂/hybrid solar cell in Fig. 2b indicates the transfer path of electrons from P3HT to PCBM to TiO₂ NRs to FTO electrode, and the holes from P3HT to PEDOT to Ag electrode. In order to elucidate the impacts of single crystal rutile TiO₂ NRs on the power conversion efficiency, reference solar cells based on TiO₂ DF was prepared using the same fabrication procedure under identical fabrication conditions. Figure 1e shows the top view SEM image of TiO₂ DF. The TiO₂ nanocrystals were well packed on the surface of FTO substrate, and the TiO₂ dense film was so thin that the surface morphology of the FTO substrate was not obscured at all.

Figure 3a compares the UV–Vis transmission spectra of TiO₂ NRs 1, TiO₂ NRs 2 and TiO₂ DF. Both TiO₂ NRs 1 and TiO₂ DF film show good transparency, with almost 90% transmittance of incident light at wavelengths longer

Fig. 1 a, c and e The top-view SEM images of TiO₂ NRs grown at 150 °C for 85 min (TiO₂ NRs 1), 100 min (TiO₂ NRs 2), and TiO₂ dense film (TiO₂ DF), respectively. b and d The tilted cross-section views of TiO₂ NRs 1 and TiO₂ NRs 2 film. The scale bars in a, b, c, d and e are all 100 nm. f XRD patterns of the TiO₂ NRs on FTO substrate



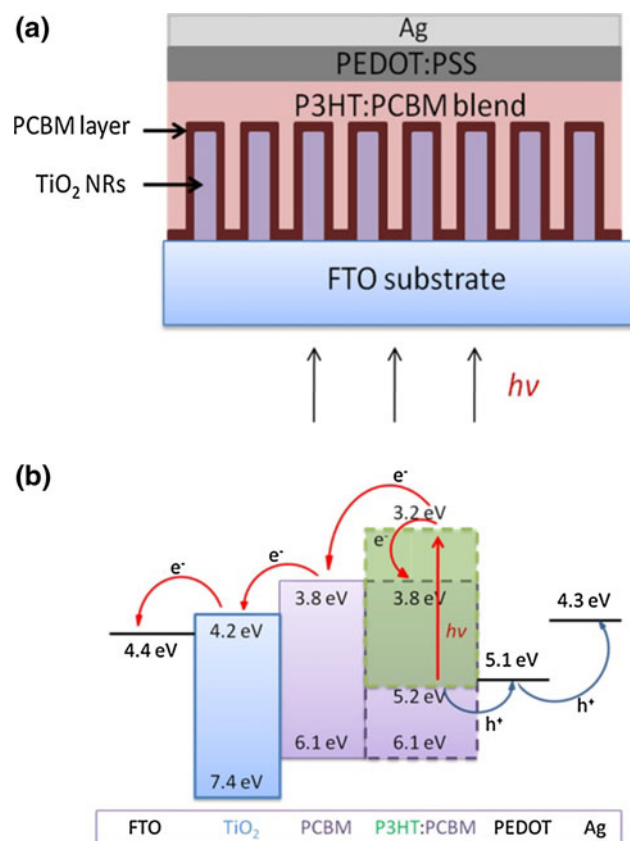


Fig. 2 a Schematic of the hybrid solar cell based on TiO_2 NRs. b Energy level diagram of TiO_2 /hybrid solar cell

than 400 nm. However, TiO_2 NRs 2 with lengths of 500 nm shows a significant loss of transmittance presumably due to light scattering, resulting in merely 50% light (at the wavelength of 500 nm) transmitting through the TiO_2 NRs 2. The transmittance decreases with the increase of diameter and height of nanorods. Thus, a much less light will be transmitted through the longer lengths TiO_2 NRs to be available for the active polymer layer to absorb. Figure 3b compares the transmission spectra of polymer embedded with TiO_2 NRs 1, TiO_2 NRs 2 and TiO_2 DF. The significantly decreased transmittance, particularly at the wavelength below 675 nm, corresponds to the intrinsic absorption of polymer between 400 and 650 nm [8, 22]. The active polymer layer in TiO_2 NRs hybrid solar cells included two parts: (1) a layer infiltrated between the TiO_2 nanorods and (2) a layer on top of the TiO_2 nanorods. Polymer embedded with TiO_2 NRs 1 shows lower transmittance than polymer coated on the TiO_2 DF, indicating the higher light absorption of polymer layer in TiO_2 NRs 1. The enhancement could be mainly due to the increased thickness of the active polymer layer as part of the polymer infiltrated into the TiO_2 NRs 1. Regardless of the much higher optical transmittance of TiO_2 NRs 1 compared with TiO_2 NRs 2 (shown in Fig. 3a), polymer embedded with

TiO_2 NRs 1 and TiO_2 NRs 2 show the similar transmittance. The increased thickness of active layer infiltrated in TiO_2 NRs 2 may improve the absorption of photons.

Figure 4 shows the I–V curves of the hybrid solar cells based on TiO_2 NRs and TiO_2 DF, with characteristic data summarized in Table 1. The best performance achieved in the hybrid solar cells based on TiO_2 NRs was open-circuit voltage (V_{oc}) = 0.595 V, short-circuit current density (J_{sc}) = 10.06 mA/cm^2 , fill factor (FF) = 0.536, and PCE = 3.21%, while the reference hybrid solar cells based on TiO_2 DF shows a PCE of 2.79%. The enhanced power conversion efficiency with TiO_2 NRs 1 resulted largely from the increased J_{sc} , suggesting an increased amount of electron–hole pairs generated, and/or a reduction of charge recombination. Hybrid solar cells based on TiO_2 NRs 1 have an higher light absorption compared to TiO_2 DF hybrid solar cells, as shown in Fig. 3b, leading to the enhancement of generated electron–hole pairs. The single crystal TiO_2 NRs with high electron mobility, penetrated in

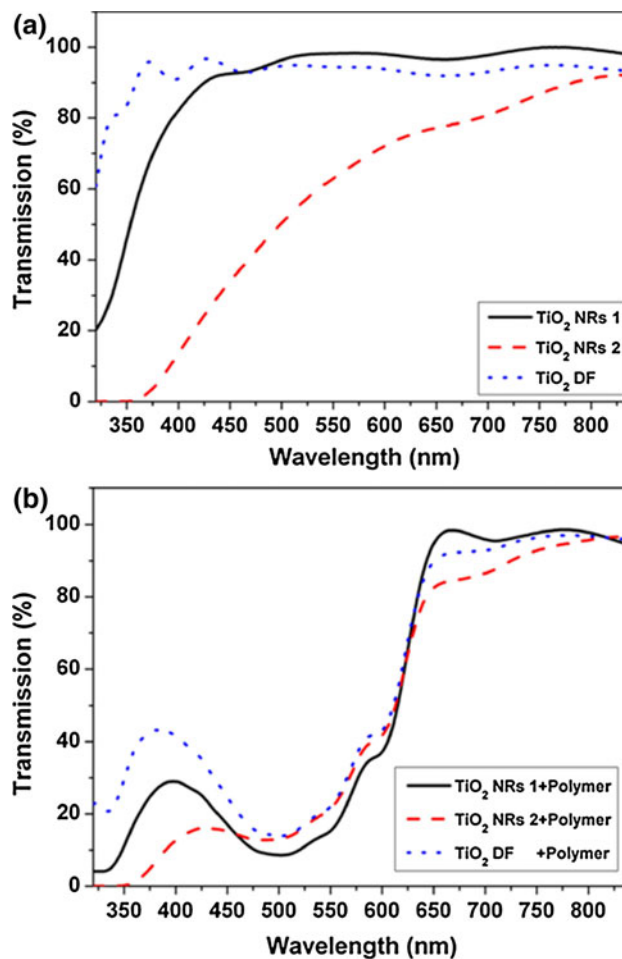


Fig. 3 a Transmission spectrum of TiO_2 NRs grown at 150 °C for 85 min (TiO_2 NRs 1), 100 min (TiO_2 NRs 2) and the compared TiO_2 dense film (TiO_2 DF). b Transmission spectrum of PCBM/P3HT:PCBM embedded with TiO_2 NRs 1, TiO_2 NRs 2 and TiO_2 DF film

the active polymer layer would also function as the direct pathway for the quick electron transport to the charge collecting electrode, leading to efficient charge collection and reduced charge recombination. It is worth noting that the reference TiO₂ DF electrode used in this work was anatase phase, which was different from the TiO₂ NRs in rutile phase. It is well known [23, 24] that anatase TiO₂ exhibits significantly higher diffusion coefficient of conduction band electrons and greater electron mobility than the rutile phase, which would benefit for high power conversion efficiency. In other words, if the TiO₂ NRs were in anatase phase, a much higher power conversion efficiency would be achieved than that in the present study with the TiO₂ NRs in rutile phase, further reinforces the observation that the nanorods enhance the power conversion efficiency. It also suggests further study on the preparation of single-crystalline anatase TiO₂ NRs and their application in hybrid solar cells. The hybrid solar cell based on TiO₂ NRs 2 demonstrated a much lower PCE than the one based on TiO₂ NRs 1, probably due to the lower light absorption of polymer embedded TiO₂ NRs 2 and the longer distance for the electron transport to the charge collecting electrode. The PCE of the solar cells based on TiO₂ NRs 2 can be achieved 5.07% when normalized to the incident light that transmitted through the TiO₂ NRs 2 at the intrinsic absorption range of polymer between 400 nm and 650 nm. The result suggests that the hybrid solar cells based on long lengths TiO₂ NRs could significantly enhance the power conversion efficiency if the transparency of TiO₂ NRs can be improved.

Figure 5 shows atomic force microscopy (AFM) topography of polymer-blend TiO₂ NRs 1 (Fig. 5a) and TiO₂ NRs 2 (Fig. 5b). The surface roughness (rms) of the active polymer layer increases with the increased lengths of

nanorods, changing from 4.32 nm for TiO₂ NRs 1 to 24.08 nm for TiO₂ NRs 2. The active layer with a larger roughness would have poor contact with the silver electrode, leading to less efficient hole collection and resulting in lower PCE. In addition, if TiO₂ NRs are not well

Table 1 The performances of the hybrid solar cells based on TiO₂ NRs 1, TiO₂ NRs 2 and TiO₂ DF

Samples	V _{oc} (V)	J _{sc} (mA/cm ²)	FF	η (%)
TiO ₂ NRs 1	0.595	10.06	0.536	3.21
TiO ₂ NRs 2	0.580	9.05	0.513	2.70
TiO ₂ DF	0.589	8.80	0.538	2.79

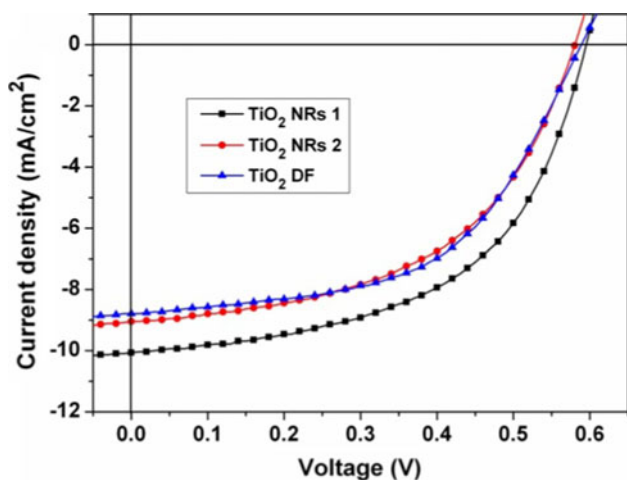


Fig. 4 I-V curves of the hybrid solar cells based on TiO₂ NRs 1, TiO₂ NRs 2 and TiO₂ DF under AM 1.5 G illumination at 100 mW/cm²

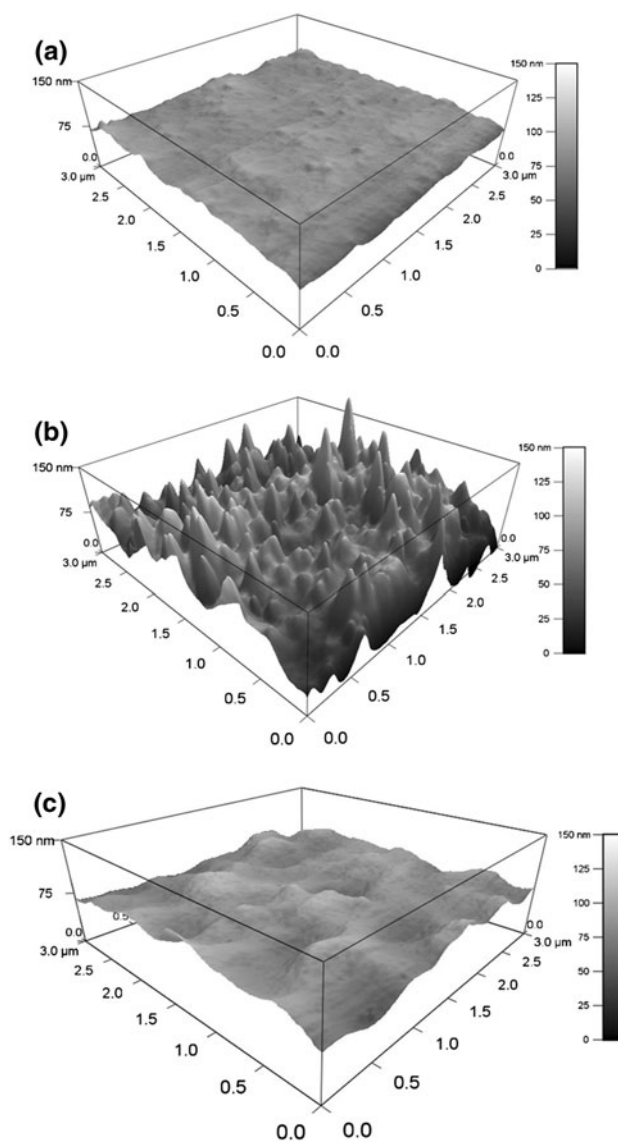


Fig. 5 AFM topography of the polymer surface (P3HT/PCBM) embedded with TiO₂ NRs with different lengths: **a** TiO₂ NRs 1, **b** TiO₂ NRs 2 and **c** TiO₂ NRs 2-DL

covered with active polymer blend, there will be a noticeable current leakage [1]. Figure 6 shows the cross-section SEM images of the polymer blend TiO₂ NRs 1 (Fig. 6a) and TiO₂ NRs 2 (Fig. 6b). The thickness of entire active layer is 270 nm for TiO₂ NRs 1 and 500 nm for TiO₂ NRs 2. The thickness of the active layer on TiO₂ NRs 2 is similar to the lengths of TiO₂ NRs 2, as shown in Fig. 1d, which indicates the polymer has penetrated to the gaps between nanorods, but is insufficient to well cover nanorods.

To improve the surface morphology and ensure the full coverage of active polymer layer on TiO₂ NRs 2, two layers of the P3HT/PCBM blend solution were spin coated under the same condition, labeled as TiO₂ NRs 2-DL. AFM and SEM were also applied to exam the surface morphology of polymer-blend TiO₂ NRs 2-DL. Polymer-blend TiO₂ NRs 2-DL shows the smaller hillocks and smoother surface, with much reduced surface roughness of 7.58 nm (shown in Fig. 5c), compared to polymer-blend TiO₂ NRs 2 with only one layer P3HT/PCBM coating. Figure 6c shows the cross-section image of polymer-blend TiO₂ NRs 2-DL. The thickness of the active layer increased to 610 nm, which suggests the improved coverage of polymer

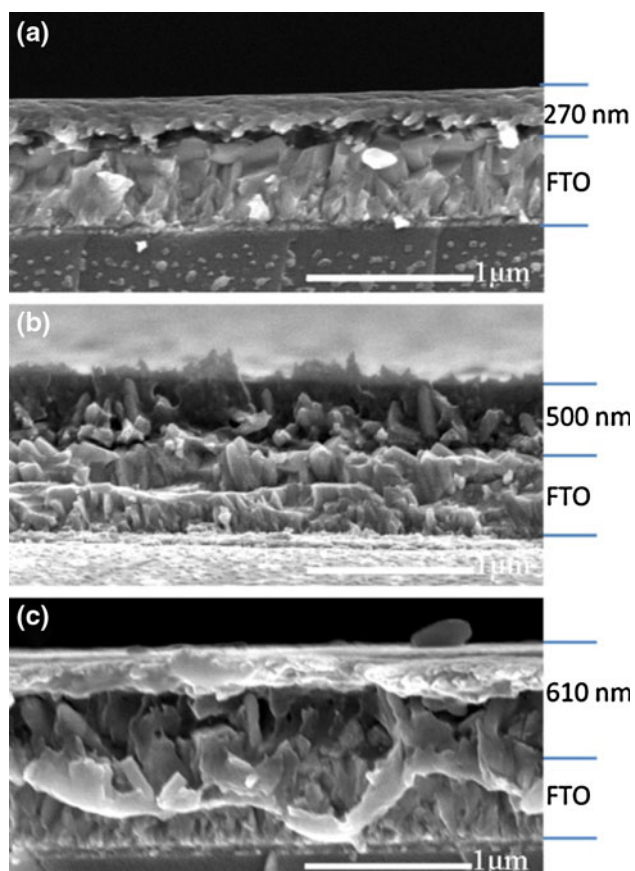


Fig. 6 SEM cross-sections of polymer blend TiO₂ NRs films: **a** TiO₂ NRs 1, **b** TiO₂ NRs 2 and **c** TiO₂ NRs 2-DL

coatings on the surface of TiO₂ nanorods. Hybrid solar cells based on TiO₂ NRs 2-DL can achieve a PCE of 3.07%, with $V_{oc} = 0.622$ V, $J_{sc} = 9.71$ mA/cm², and $FF = 0.509$. This result strongly suggests that the bilayer structured coating of active polymer blend is very promising to improve the performance of hybrid solar cells with long lengths nanorods.

4 Conclusions

In summary, single-crystal rutile TiO₂ nanorods were grown directly on FTO substrate by means of hydrothermal method. This approach is simple and straight for the TiO₂ nanorods growth without using templates or seeds. The hybrid solar cells based on such single crystal rutile TiO₂ NRs demonstrated a much enhanced PCE of 3.21%; an even higher PCE would be achieved if single crystal anatase TiO₂ NRs can be synthesized and used. Single crystal rutile TiO₂ NRs are believed to function as direct pathways for easy electron transport and less charge recombination. Much higher power conversion efficiency with long TiO₂ nanorods would be obtained, if light transmittance through TiO₂ NRs could be improved, or the incident light is introduced from the opposite side of the TiO₂ nanorods. In addition, when bilayer structured polymer coating was applied into the long TiO₂ nanorods, the contact between the polymer blend and silver electrode was improved and the surface roughness of active polymer layer was reduced, resulting in an enhanced PCE.

Acknowledgments JTX gratefully acknowledges the fellowship from China Scholarship Council. And this work has been supported in part by National Natural Science Foundation of China (21173042), Natural Science Foundation of Jiangsu Province (BK2011589), the US Department of Energy, Office of Basic Energy Sciences, Division of Materials and Engineering under Award No. DE-FG02-07ER46467 (Q.F.Z.) on the microstructure characterization and some power conversion efficiency measurements, National Science Foundation (DMR-1035196), Boeing-Steiner Endowment, University of Washington TGIF grant and Intel Corporation. The AFM analysis was performed at Prof. Jiangyu Li's laboratory, Department of Mechanical Engineering, University of Washington. ZQL and OW also acknowledge the fellowship from China Scholarship Council and Thailand government, respectively.

References

1. C.Y. Kuo, C. Gau, *Appl. Phys. Lett.* **95**, 053302 (2009)
2. E.D. Spoeke, M.T. Lloyd, E.M. McCready, D.C. Olson, Y.J. Lee, J.W.P. Hsu, *Appl. Phys. Lett.* **95**, 213506 (2009)
3. C.H. Hsieh, Y.J. Cheng, P.J. Li, C.H. Chen, M. Dubosc, R.M. Liang, C.S. Hsu, *J. Am. Chem. Soc.* **132**, 4887 (2010)
4. H. Hoppe, M. Niggemann, C. Winder, J. Kraut, R. Hiesgen, A. Hinsch, D. Meissner, N.S. Sariciftci, *Adv. Funct. Mater.* **14**, 1005 (2004)

5. S. Gunes, H. Neugebauer, N.S. Sariciftci, *Chem. Rev.* **107**, 1324 (2007)
6. H. Hoppe, N.S. Sariciftci, *J. Mater. Chem.* **16**, 45 (2006)
7. Y.Y. Liang, Z. Xu, J.B. Xia, S.T. Tsai, Y. Wu, G. Li, C. Ray, L.P. Yu, *Adv. Mater.* **22**, E135 (2010)
8. P.Y. Yang, X.Y. Zhou, G.Z. Cao, C.K. Luscombe, *J. Mater. Chem.* **20**, 2612 (2010)
9. S. Yodyingyong, X.Y. Zhou, Q.F. Zhang, D. Triampo, J.T. Xi, K. Park, B. Limketkai, G.Z. Cao, *J. Phys. Chem. C* **114**, 21851 (2010)
10. G. Li, V. Shrotriya, J.S. Huang, Y. Yao, T. Moriarty, K. Emery, Y. Yang, *Nat. Mater.* **4**, 864 (2005)
11. W.L. Ma, C.Y. Yang, X. Gong, K. Lee, A.J. Heeger, *Adv. Funct. Mater.* **15**, 1617 (2005)
12. C.Y. Kuo, W.C. Tang, C. Gau, T.F. Guo, D.Z. Jeng, *Appl. Phys. Lett.* **93**, 033307 (2008)
13. Y.C. Huang, W.C. Yen, Y.C. Liao, Y.C. Yu, C.C. Hsu, M.L. Ho, P.T. Chou, W.F. Su, *Appl. Phys. Lett.* **96**, 123501 (2010)
14. T. Ishwara, D.D.C. Bradley, J. Nelson, P. Ravirajan, I. Vanseveren, T. Cleij, D. Vanderzande, L. Lutsen, S. Tierney, M. Heeney, I. McCulloch, *Appl. Phys. Lett.* **92**, 053308 (2008)
15. J.S. Huang, C.Y. Chou, C.F. Lin, *Sol. Energy Mater. Sol. Cells* **94**, 182 (2010)
16. S.K. Hau, H.L. Yip, A.K.Y. Jen, *Polym. Rev.* **50**, 474 (2010)
17. K. Takanezawa, K. Hirota, Q.S. Wei, K. Tajima, K. Hashimoto, *J. Phys. Chem. C* **111**, 7218 (2007)
18. Q.S. Wei, K. Hirota, K. Tajima, K. Hashimoto, *Chem. Mater.* **18**, 5080 (2006)
19. B. Liu, E.S. Aydil, *J. Am. Chem. Soc.* **131**, 3985 (2009)
20. A. Kumar, A.R. Madaria, C.W. Zhou, *J. Phys. Chem. C* **114**, 7787 (2010)
21. X.J. Feng, K. Shankar, O.K. Varghese, M. Paulose, T.J. Latempa, C.A. Grimes, *Nano Lett.* **8**, 3781 (2008)
22. B.Y. Yu, A. Tsai, S.P. Tsai, K.T. Wong, Y. Yang, C.W. Chu, J.J. Shyue, *Nanotechnology* **19**, 255202 (2008)
23. N.A. Deskins, M. Dupuis, *Phys. Rev. B* **75**, 195212 (2007)
24. S. Kambe, S. Nakade, Y. Wada, T. Kitamura, S. Yanagida, *J. Mater. Chem.* **12**, 723 (2002)